APCOM'07 in conjunction with EPMESC XI, *December 3-6, 2007, Kyoto, JAPAN*

On the Convergence of the Kriging-based Finite Element Method

Foek Tjong Wong*, Worsak Kanok-Nukulchai

School of Engineering and Technology, Asian Institute of Technology, P.O. Box 4, Klong Luang, Pathumthani, 12120, Thailand
e-mail: st100127@ait.ac.th, worsak@ait.ac.th

Abstract An enhancement of the finite element method using Kriging shape functions (K-FEM) was recently proposed. Since then the K-FEM has been improved and applied to solve various problems in continuum mechanics. This method is as simple as the conventional FEM in view of the formulation and implementation and yet it is as flexible as mesh-free methods in term of customizing the interpolation function for a desired degree of consistency. However, the interpolation function between two boundary nodes is not fully closed. This causes incompatibility and consequently the convergence of the solutions is questionable. In this paper, the convergence characteristics of the K-FEM with different options of the basis function, number of layers and correlation function were scrutinized through a series of weak patch tests for plane stress and Reissner-Mindlin plate problems. In addition, a benchmark plane stress problem was solved to illustrate the convergence of the method with various options. A relative L_2 norm of error or relative error of strain energy was used to measure the accuracy. The results reveal that the K-FEM passes the weak patch tests for most of the options. Basically, the incompatibility in the K-FEM tends to decrease as the mesh is refined. The K-FEM with quartic spline correlation function generally has better convergence characteristic than that with the Gaussian.

Key words: finite element, Kriging, convergence, patch test, Reissner-Mindlin

INTRODUCTION

In the past two decades various mesh-free methods have been developed and applied to solve problems in continuum mechanics (e.g., see [1], [2]). These methods have drawn attentions of many researchers partly due to their flexibility in customizing the approximation function for desired accuracy. Of all the mesh-free methods, the methods using the Galerkin weak form such as the element-free Galerkin method (EFGM) [3] and point interpolation methods [1: pp.250-300] have the same basic formulation with FEM. Although the EFGM and its variants have appeared in many academic articles for more than a decade, up to now they seem to find little acceptance in real practice. This is in part due to the inconvenience in their implementation, such as difficulties in constructing mesh-free approximations for highly irregular problem domains and in handling problems of material discontinuity [1: pp.15 and 644].

A very convenient implementation of EFGM was recently proposed [4]. Following the work of Gu [5], Kriging interpolation (KI) was used as the trial function. Since KI passing through the nodes (posses the Kronecker delta property), there is no need for special treatment of boundary conditions. For evaluating the integrals in the Galerkin weak form, finite elements were used as the integration cells. The KI was constructed for each element by the use of a set of nodes in a domain of influence (DOI) composed of several layers of elements (the DOI is in the form of polygon for 2D problems). With this way of implementation, the EGFM of Plengkhom and Kanok-Nukulchai [4] can be viewed as a subclass of FEM with Kriging shape functions. This method is referred to as Kriging-based FEM (K-FEM) in this paper. The K-FEM retains the advantages of mesh-free methods as follows:

1. Any requirement for high order shape functions can be easily fulfilled without any change to the element structure.

2. The field variables and their derivatives can be obtained with remarkable accuracy and global smoothness.

A distinctive advantage of the K-FEM over other mesh-free methods is that it inherits the computational procedure of FEM so that existing general-purpose FE programs can be easily extended to include this new method. Thus, the K-FEM has a higher change to be accepted in practical applications.

In the K-FEM, the interpolation functions are not continuous (*incompatible*) along the interfaces of elements [6, 7] due to the possible opening of the support edges along nodal intervals. Due to this incompatibility, doubt on the convergence of the method naturally comes up. However, the convergence of the K-FEM has not been studied in the previous literature [4, 8]. In the present paper, the convergence of the method was scrutinized by means of a series of *weak* patch tests for plane stress and Reissner-Mindlin plate problems. A relative L_2 norm of error or relative error of strain energy was used to measure the accuracy. Detail studies on convergence characteristics of the K-FEM with different options of the basis function, number of layers and correlation function were performed. In addition, an example of benchmark plane stress problem was used to illustrate the convergence of various versions of the K-FEM. It is the intention of this paper to assess the convergence of the K-FEM with different options.

KRIGING INTERPOLATION

This section presents a review of the KI formulation in the context of K-FEM. A detail explanation and derivation of Kriging may be found in References [6, 7, 9, 10].

Formulation

Consider a continuous field variable $u(\mathbf{x})$ defined in a domain Ω. The domain is represented by a set of properly scattered nodes $\mathbf{x}_i$, i=1, 2, …, N, where N is the total number of nodes in the whole domain. Given N field values $u(\mathbf{x}_1)$, …, $u(\mathbf{x}_N)$, the problem is to obtain an estimate value of u at a point $\mathbf{x}_0 \in \Omega$.

The Kriging estimated value $u^{\mathrm{h}}(\mathbf{x}_0)$ is a linear combination of $u(\mathbf{x}_1)$, …, $u(\mathbf{x}_n)$, i.e.

$$u^{\mathrm{h}}(\mathbf{x}_0) = \sum_{i=1}^{n} \lambda_i u(\mathbf{x}_i) \tag{1}$$

where λ_i's are termed as (*Kriging*) *weights* and n is the number of nodes surrounding point $\mathbf{x}_0$ inside a sub-domain $\Omega_{\mathbf{x}0} \subseteq \Omega$. This sub-domain is referred to as *domain of influence* (DOI) in this paper. Considering each function values $u(\mathbf{x}_1)$, …, $u(\mathbf{x}_n)$ as the realizations of random variables $U(\mathbf{x}_1)$, …, $U(\mathbf{x}_n)$, Eq. (1) can be written as

$$U^{\mathrm{h}}(\mathbf{x}_0) = \sum_{i=1}^{n} \lambda_i U(\mathbf{x}_i) \tag{2}$$

The Kriging weights are determined by requiring the estimator $U^{\mathrm{h}}(\mathbf{x}_0)$ is *unbiased*, i.e.

$$\mathrm{E}\left[U^{\mathrm{h}}(\mathbf{x}_0) - U(\mathbf{x}_0)\right] = 0 \tag{3}$$

and *by minimizing* the variance of estimation error, $\mathrm{var}\left[U^{\mathrm{h}}(\mathbf{x}_0) - U(\mathbf{x}_0)\right]$. Using the method of Lagrange for constraint optimization problems, the requirements of minimum variance and unbiased estimator lead to the following Kriging equation system:

$$\mathbf{R}\boldsymbol{\lambda} + \mathbf{P}\boldsymbol{\mu} = \mathbf{r}(\mathbf{x}_0) \tag{4a}$$

$$\mathbf{P}^{\mathrm{T}}\boldsymbol{\lambda} = \mathbf{p}(\mathbf{x}_0) \tag{4b}$$

in which

$$\mathbf{R}=\begin{bmatrix} C(\mathbf{h}_{11}) & \dots & C(\mathbf{h}_{1n}) \\ \dots & \dots & \dots \\ C(\mathbf{h}_{n1}) & \dots & C(\mathbf{h}_{nn}) \end{bmatrix};\quad \mathbf{P}=\begin{bmatrix} p_1(\mathbf{x}_1) & \dots & p_m(\mathbf{x}_1) \\ \dots & \dots & \dots \\ p_1(\mathbf{x}_n) & \dots & p_m(\mathbf{x}_n) \end{bmatrix}; \tag{4c}$$

$$\boldsymbol{\lambda}=\begin{bmatrix}\lambda_1 & \dots & \lambda_n\end{bmatrix}^{\mathrm{T}};\quad \boldsymbol{\mu}=\begin{bmatrix}\mu_1 & \dots & \mu_m\end{bmatrix}^{\mathrm{T}} \tag{4d}$$

$$\mathbf{r}(\mathbf{x}_0)=\begin{bmatrix}C(\mathbf{h}_{10}) & C(\mathbf{h}_{20}) & \dots & C(\mathbf{h}_{n0})\end{bmatrix}^{\mathrm{T}};\quad \mathbf{p}(\mathbf{x}_0)=\begin{bmatrix}p_1(\mathbf{x}_0) & \dots & p_m(\mathbf{x}_0)\end{bmatrix}^{\mathrm{T}} \tag{4e}$$

$\mathbf{R}$ is $n\times n$ matrix of covariance between $U(\mathbf{x})$ at nodes $\mathbf{x}_1, \dots, \mathbf{x}_n$; $\mathbf{P}$ is $n\times m$ matrix of polynomial values at the nodes; $\boldsymbol{\lambda}$ is $n\times 1$ vector of Kriging weights; $\boldsymbol{\mu}$ is $m\times 1$ vector of Lagrange multipliers; $\mathbf{r}(\mathbf{x}_0)$ is $n\times 1$ vector of covariance between the nodes and the node of interest, $\mathbf{x}_0$; and $\mathbf{p}(\mathbf{x}_0)$ is $m\times 1$ vector of polynomial basis at $\mathbf{x}_0$. In Eqs. (4c) and (4e), $C(\mathbf{h}_{ij})=\mathrm{cov}\left[U(\mathbf{x}_i),U(\mathbf{x}_j)\right]$. Kriging weights $\boldsymbol{\lambda}$ are obtained by solving the Kriging equations, Eqs. (4a) and (4b).

The expression for the estimated value u^{h} given by Eq. (1) can be rewritten in matrix form,

$$u^{\mathrm{h}}(\mathbf{x}_0)=\boldsymbol{\lambda}^{\mathrm{T}}\mathbf{d} \tag{5}$$

where $\mathbf{d}=\begin{bmatrix}u(\mathbf{x}_1) & \dots & u(\mathbf{x}_n)\end{bmatrix}^{\mathrm{T}}$ is $n\times 1$ vector of nodal values. Since the point $\mathbf{x}_0$ is an arbitrary point in the DOI, the symbol $\mathbf{x}_0$ can be replaced by symbol $\mathbf{x}$. Thus, using the usual finite element terminology, Eq. (5) can be expressed as

$$u^{\mathrm{h}}(\mathbf{x})=\mathbf{N}(\mathbf{x})\mathbf{d}=\sum_{i=1}^{n}N_i(x)u_i \tag{6}$$

in which $\mathbf{N}(\mathbf{x})=\boldsymbol{\lambda}^{\mathrm{T}}(\mathbf{x})$.

Two key properties of Kriging shape functions that make them appropriate to be used in the FEM are *Kronecker delta* (or *interpolation*) property and *consistency* property [5, 6]. Due to the former property KI exactly passes through the nodal values. The consequence of the latter property is that if the basis includes all constants and linear terms, the Kriging shape functions are able to reproduce a linear polynomial exactly.

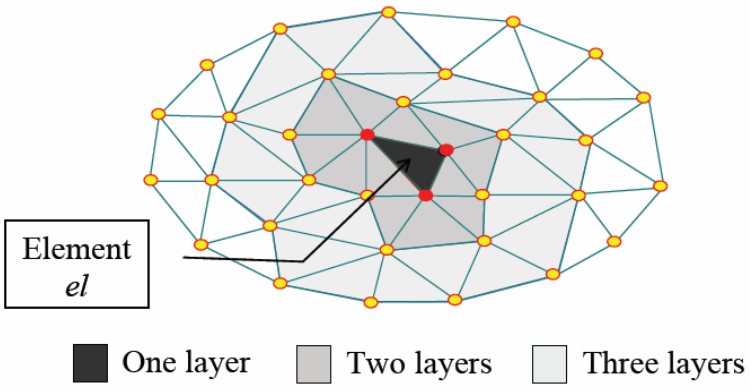

Fig. 1 Domain of influence for element el with one, two and three layers of elements [4]

Layered-Element Domain of Influence

Let us consider a 2D domain meshed with triangular elements, such as illustrated in Fig. 1. For each element, KI is constructed based upon a set of nodes in a polygonal DOI encompassing a predetermined number of layers of elements. The KI function over the element is given by Eq. (6). By combining the KI of all elements in the domain, the global field variable is approximated by piecewise KI. This way of approximation is very similar with the approximation in the conventional FEM.

Within each element the interpolation function is naturally continuous. However, along the element edges between two adjacent elements the function is not continuous because the KI for each neighboring element is constructed using different set of nodes. Thus the present method is *nonconforming*.

The number of layers for each element must cover a minimum number of nodes in such way that Kriging equation system, Eqs. (4a) and (4b), is solvable. If an *m*-order polynomial basis is employed, the DOI is required to cover a number of nodes, *n*, that is equal or greater than the number of terms in the basis function [4].

Polynomial Basis and Correlation Function

Constructing Kriging shape functions in Eq. (6) requires a polynomial basis function and a model of covariance function. For the basis function, besides complete polynomial bases, it is also possible to use incomplete polynomial bases such as bi-linear, bi-quadratic and bi-cubic bases [11].

Covariance between a pair of random variables $U(\mathbf{x})$ and $U(\mathbf{x}+\mathbf{h})$ can be expressed in terms of correlation coefficient function or shortly, *correlation function*, i.e. $\rho(\mathbf{h}) = C(\mathbf{h})/\sigma^2$, where $\sigma^2 = \mathrm{var}\left[U(\mathbf{x})\right]$. According to Gu [5], σ^2 has no effect on the final results and so in this study it is taken as 1. One of the widely used correlation model in the area of computational mechanics is the Gaussian correlation function [4-8], viz.

$$\rho(\mathbf{h}) = \rho(h) = \exp(-(\theta h/d)^2) \tag{7}$$

where θ>0 is the *correlation parameter*, $h = \|\mathbf{h}\|$, i.e. the Euclidean distance between points **x** and **x**+**h**, and *d* is a scale factor to normalize the distance. In this study, *d* is taken to be the *maximum distance* between any pair of nodes in the DOI. Besides the Gaussian, we recently introduced the quartic spline (QS) correlation function [6, 8] as follows:

$$\rho(\mathbf{h}) = \rho(h) = \begin{cases} 1-6(\theta h/d)^2+8(\theta h/d)^3-3(\theta h/d)^4 & \text{for } 0 \le \theta h/d \le 1 \\ 0 & \text{for } \theta h/d > 1 \end{cases} \tag{8}$$

Our study [6] shows that with this correlation function, Kriging shape functions are not very sensitive to the change in parameter θ.

The proper choice of parameter θ is very important because it affects the quality of KI. In order to obtain reasonable results in the K-FEM, Plengkhom and Kanok-Nukulchai [4] suggested a rule of thumb for choosing θ, i.e. θ should be selected so that it satisfies the lower bound,

$$\left|\sum_{i=1}^{n} N_i - 1\right| \le 1\times 10^{-10+a} \tag{9}$$

where *a* is the order of basis function, and also satisfies the upper bound,

$$\det(\mathbf{R}) \le 1\times 10^{-b} \tag{10}$$

where *b* is the dimension of problem. For 2D problem with cubic basis function, for example, *a*=3 and *b*=2.

Numerical investigations on the upper and lower bound values of θ [6, 8] revealed that the parameter bounds vary with respect to the number of nodes in the DOI. Based on the results of the search for the lower and upper bound values of θ satisfying Eqs. (9) and (10), we proposed explicit parameter functions for practical implementation of the K-FEM as follows:

For the Gaussian correlation parameter, the parameter function is

$$\theta = (1-f)\theta^{\text{low}} + f\theta^{\text{up}}, \quad 0 \le f \le 0.8 \tag{11a}$$

where f is a scale factor, θ^{low} and θ^{up} are the lower and upper bound functions as follows:

$$\theta^{\text{low}} = \begin{cases} 0.08286n - 0.2386 & \text{for } 3 \le n < 10 \\ \text{-8.364E - 4}\,n^2 + 0.1204n - 0.5283 & \text{for } 10 \le n \le 55 \\ 0.02840n + 2.002 & \text{for } n > 55 \end{cases} \tag{11b}$$

$$\theta^{\text{up}} = \begin{cases} 0.34n - 0.7 & \text{for } 3 \le n < 10 \\ \text{-2.484E-3}\,n^2 + 0.3275n - 0.2771 & \text{for } 10 \le n \le 55 \\ 0.05426n + 7.237 & \text{for } n > 55 \end{cases} \tag{11c}$$

For the QS correlation parameter, the parameter function is

$$\theta = \begin{cases} 0.1329n - 0.3290 & \text{for } 3 \le n < 10 \\ 1 & \text{for } n \ge 10 \end{cases} \tag{12}$$

NUMERICAL TESTS

To study the convergence of the present K-FEM, two measures of error were utilized. The fist one is relative L_2 norm error of displacement and the second one is relative strain energy error. They are defined as follows:

$$r_u = \left(\frac{\int_V (\mathbf{u}^{\text{app}} - \mathbf{u}^{\text{exact}})^{\text{T}} (\mathbf{u}^{\text{app}} - \mathbf{u}^{\text{exact}})\, dV}{\int_V (\mathbf{u}^{\text{exact}})^{\text{T}} \mathbf{u}^{\text{exact}}\, dV} \right)^{1/2} \quad ; \quad r_\varepsilon = \left(\frac{\int_V (\boldsymbol{\varepsilon}^{\text{app}} - \boldsymbol{\varepsilon}^{\text{exact}})^{\text{T}} \mathbf{E} (\boldsymbol{\varepsilon}^{\text{app}} - \boldsymbol{\varepsilon}^{\text{exact}})\, dV}{\int_V (\boldsymbol{\varepsilon}^{\text{exact}})^{\text{T}} \mathbf{E} \boldsymbol{\varepsilon}^{\text{exact}}\, dV} \right)^{1/2} \tag{13}$$

In this equation, $\mathbf{u}^{\text{app}}$ and $\mathbf{u}^{\text{exact}}$ are approximate and exact displacement vectors, respectively, and $\boldsymbol{\varepsilon}^{\text{app}}$ and $\boldsymbol{\varepsilon}^{\text{exact}}$ are approximate and exact strain vectors, respectively. For computing these relative errors, the 13-point quadrature rule for triangles was employed for each element.

Element stiffness matrices were computed using the 6-point quadrature rule for triangles. The 6-point rule was elected because it can give reasonably accurate results yet inexpensive in terms of computational cost. For computing the nodal force vector in plane stress problems, the 2-point Gaussian quadrature for line integral was used. In Reissner-Mindlin plate problems, element nodal force vectors were computed using the 6-point quadrature rule.

Abbreviations in the form of P*-*-G* or P*-*-QS, in which the star denotes a number, were adopted in this section to designate various options of the K-FEM. The first part of the abbreviation denotes polynomial basis with the order indicated by the number next to letter P. The middle part denotes number of layers. The last part, G* denotes the Gaussian correlation function with the adaptive parameter given by Eq. (11a) and with the scale factor f indicated by the number next to letter G (in percent); QS denotes the quartic spline correlation function with the adaptive parameter given by Eq. (12). For example, P3-3-G50 means cubic basis, 3 element-layers, Gaussian correlation function with mid-value parameter function, i.e. f=0.5.

Weak Patch Tests for Plane Stress Problems

Patch test is a test to a "patch" of finite elements with states of constant strains or constant stresses. Since the K-FEM is nonconforming, it will not pass the patch test for a patch with a large size of elements. Passing the patch test for a large size of elements, however, is not a necessary condition for convergence. The *necessary* and *sufficient* condition for convergence is to pass the patch test in the limit, as the size of the elements in the patch tends to zero [12: p.254, 13], provided that the system of equations is solvable and all integrations are exact. This kind of test is referred to as *weak patch test* [12: pp.250-275, 14: p.240].

The patch used in this test is a rectangular domain of 0.24 by 0.12 with modulus of elasticity E=10^6 and Poisson's ratio v=0.25. It was adopted from the patch proposed by MacNeal and Harder [15]. For plane stress condition, force boundary conditions as shown in Fig. 2 were used. In order to be consistent with displacement field $u = 10^{-3}(x + y/2)$, $v = 10^{-3}(y + x/2)$, $u = 0.24\times10^{-3}$ and $v = 0.12\times10^{-3}$ were prescribed at node B. The initial course mesh, which includes 25 nodes, is shown in Fig.3. We define the element characteristic size for this mesh h_c=0.06. Subsequently, mesh refinements were performed by subdividing the elements.

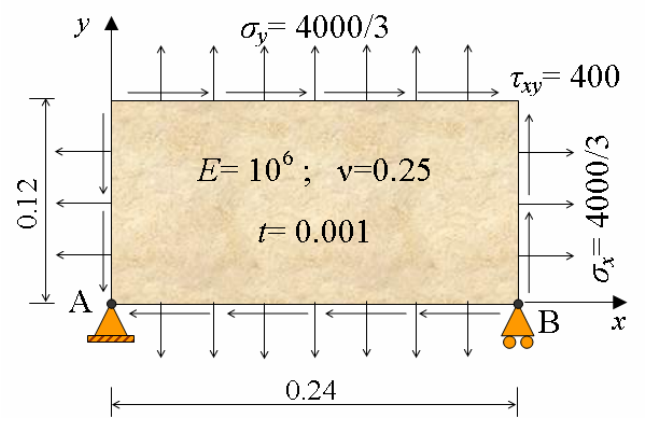

Fig. 2 A patch under constant stress

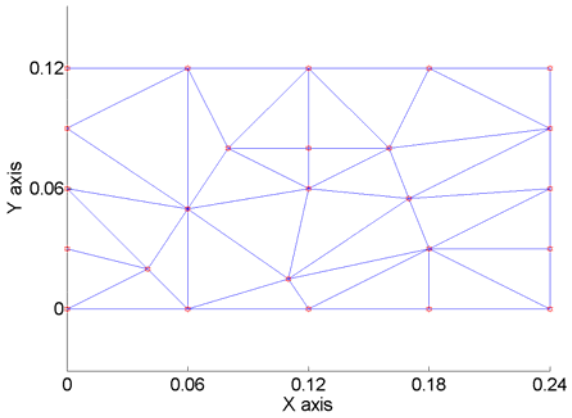

Fig. 3 Initial mesh of the domain for weak patch test

The following K-FEM options were elected for the weak patch test: P2-2 with G0, G50, G80, QS and P3-3 with G0, G50, G80, QS. Displacement error norms of the K-FEM solutions were plotted against element characteristic sizes in Fig. 4. The average convergence rate (R) of each option was also shown in the legends. The figure shows that the K-FEM does not pass the test in any mesh but the solutions converge. For the K-FEM of option P3-3-G0, however, the convergence is doubtful. Therefore, we conclude that the K-FEM *passes the weak patch test*, except that with option P3-3-G0. For the K-FEM with Gaussian correlation functions, as the parameter θ comes closer to the upper bound values, the convergence rate and accuracy increase. The K-FEM with the QS is the best in term of convergence rate (R=1.45 for P2-2 and R=1.82 for P3-3).

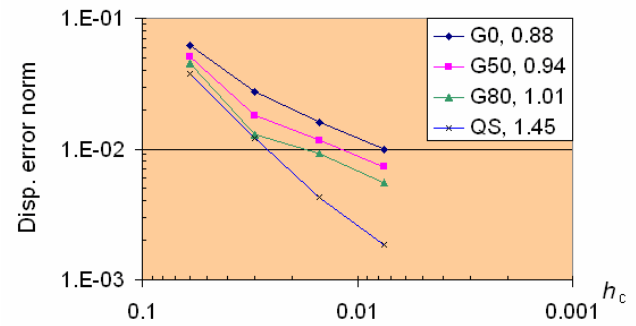

(a) P2-2

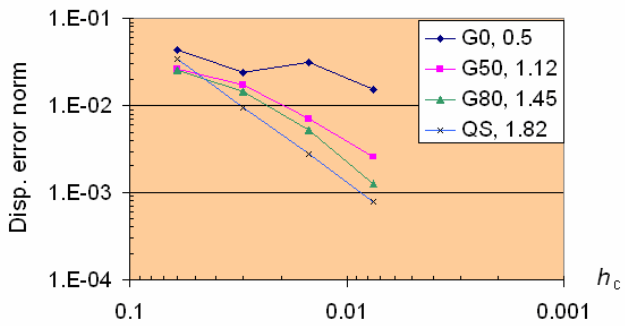

(b) P3-3

Fig. 4 Relative L_2 norm errors of displacement and convergence rates for the patch analyzed using the K-FEM with: (a) P2-2, (b) P3-3. The number after the code for K-FEM option in the legend indicates the average convergence rate.

The strain energy error norms vs. element characteristic sizes were shown in Fig. 5. These energy errors are mainly due to "gaps" or "overlaps" along the interface between two elements because the round-off and numerical integration errors are negligible. Therefore, in this case the energy error may serve as a measure of the degree of incompatibility of the K-FEM. The figure shows that the incompatibilities of the

K-FEM with various options tend to decrease as the mesh was refined. The K-FEM with QS correlation function is "more compatible" than that with the Gaussian.

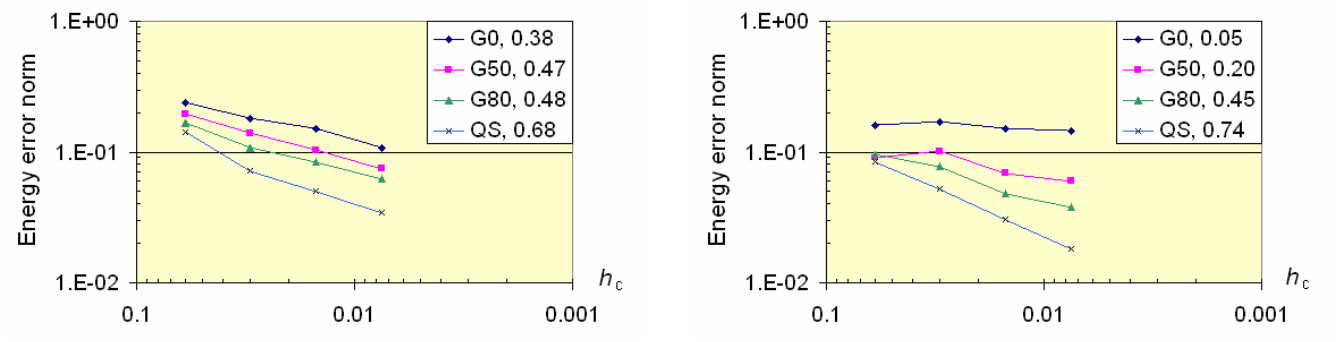

(a) P2-2 (b) P3-3

Fig. 5 Relative strain energy errors and convergence rates for the patch analyzed using the K-FEM with: (a) P2-2, (b) P3-3

Weak Patch Tests for Reissner-Mindlin Plates

The same patch and meshes were used in the following tests. Two conditions of the patch were considered, namely (1) constant curvature and (2) constant transverse shear strain. The length-to-thickness ratio of the patch was differently specified for each condition of the tests. Based on the study on the performance of various K-FEM options in alleviating shear locking [16], the following K-FEM options were elected for the patch tests: P3-3-G0, P3-3-QS, P4-4-G0, and P4-4-QS.

Constant curvature condition

The boundary of the patch was imposed by the essential boundary conditions as presented in MacNeal and Harder [15], i.e.

$$w = 10^{-3}(x^2 + xy + y^2)/2 \;;\quad \psi_x = \partial w/\partial x = 10^{-3}(x + y/2) \;;\quad \psi_y = \partial w/\partial y = 10^{-3}(x/2 + y) \tag{14}$$

where w, ψ_x and ψ_x represent the deflection, rotations with respect to the $-y$ and x directions, respectively. These fields lead to the following constant curvatures and moments:

$$\boldsymbol{\kappa} = \{1 \quad 1 \quad 1\}^{\mathrm{T}} \times 10^{-3} \;;\quad \mathbf{M} = -\{10/9 \quad 10/9 \quad 1/3\}^{\mathrm{T}} \times 10^{-7} \tag{15}$$

Shear strains and shear stresses corresponding to these constant curvatures are zero. The length-to-thickness ratio of the patch was set to 240 (h=0.001) in order to represent thin plates.

Displacement error norms of the K-FEM solutions were plotted against element characteristic sizes in Fig. 6. It can be seen that from the second mesh (h_c =0.03) until the last mesh (h_c =0.0075) the solutions of the K-FEM converge, except for the K-FEM with option P3-3-G0. The solutions for the mesh of h_c=0.06 (25 nodes) are exceptionally accurate because 16 of the 25 nodes are located at the boundary and accordingly imposed by the boundary conditions, Eq. (14). Thus, the nodal displacements associated with the 16 boundary nodes are automatically exact. In addition, for cases of relatively small number of nodes in a domain, the K-FEM may yield extraordinary accurate results because the KI is close to a polynomial function of higher order than the basis function. We conclude that the K-FEM with options P3-3-QS, P4-4-G0, and P4-4-QS *pass* the weak constant curvature patch test but the K-FEM with P3-3-G0 does *not pass*. The K-FEM with QS correlation function has better convergence characteristic than that with G0. This finding is similar to the one in the plane stress condition.

Constant transverse shear-strain condition

A state of constant transverse shear strains and zero curvatures, i.e.

$$\boldsymbol{\varepsilon}_s = \{1 \quad 1\}^{\mathrm{T}} \times 10^{-6} \;\; ; \;\; \boldsymbol{\kappa} = \{0 \quad 0 \quad 0\}^{\mathrm{T}} \tag{16}$$

can be obtained, with all equilibrium equations satisfied, only for the extreme case of thick plates [17]. In this test, an extremely-thick plate with the length-to-thickness ratio 0.0024 (h=100) was considered. The displacement fields leading to the constant shear strains, Eq. (16), are as follows:

$$w = 10^{-6}(x+y)/2 \;\; ; \;\; \psi_x = -1/2\times 10^{-6} \;\; ; \;\; \psi_y = -1/2\times 10^{-6} \tag{17}$$

The shear forces corresponding to the constant shear strains are $\mathbf{Q} = \{100/3 \quad 100/3\}^{\mathrm{T}}$.

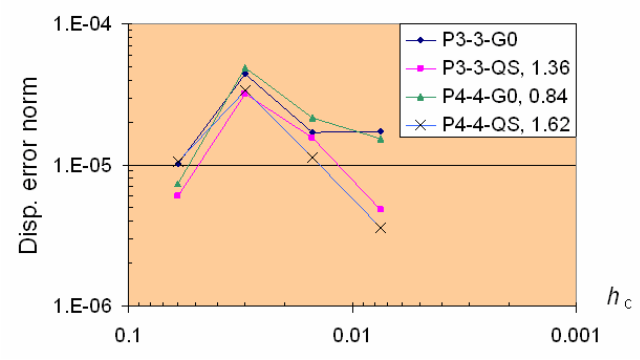

Fig. 6 Displacement error norm vs. element characteristic size for the constant curvature patch test. The numbers in the legend indicate the average convergence rates from the second mesh up to the last.

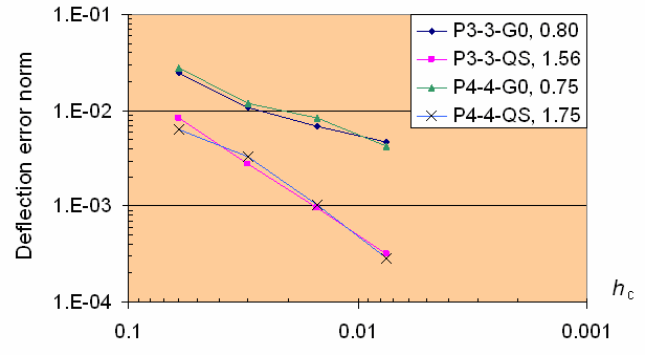

Fig. 7 Deflection error norm vs. element characteristic size for the constant shear patch test. The numbers in the legend indicate the average convergence rates.

The test was performed by imposing nodal values on the boundary according to the fields stated by Eq. (17). The error indicator used in this test is the relative L_2 norm of deflection error, defined as

$$r_w = \left(\frac{\int_S (w^{\text{app}} - w^{\text{exact}})^2 \, dS}{\int_S (w^{\text{exact}})^2 \, dS} \right)^{1/2} \tag{18}$$

This indicator was used here instead of the displacement error norm, Eq. (13), because the thickness of the plate is extremely large so that if we used the error norm of Eq. (13), the norm would be dominated by the rotation errors. We found that these rotation errors are relatively constant for different degrees of mesh refinements.

The plot of the relative deflection error norms for the K-FEM with different analysis options is shown in Fig. 7. It can be seen that all of the options lead to converging solutions and therefore they pass the weak constant shear patch test. As in the previous test, the accuracy and convergence rate of the K-FEM with QS is better than that with G0.

An Infinite Plane-stress Plate with a Hole

An infinite plane-stress plate with a circular hole of radius a=1 is subjected to a uniform tension T_x=100 at infinity [18] (Fig. 8). Owing to symmetry, only the upper right quadrant of the plate, $0 \le x \le 5$ and $0 \le y \le 5$, was analyzed. Zero normal displacements were prescribed on the symmetric boundaries and the exact traction boundary conditions were imposed on the right (x=5) and top (y=5) edges.

The initial course mesh of 42 nodes is shown in Fig. 9. The element characteristic size for this problem is taken as the distance between two nodes at the right or top edge, i.e. h_c=1. Subsequently, the mesh was refined by subdividing the previous element into four smaller elements. The refined meshes considered in this test are meshes with h_c=0.5 (141 nodes) and h_c=0.25 (513 nodes). In performing the analysis with

h_c=0.25 using Gaussian correlation function, the scale factor f=0.79 was used in place of f=0.8 because the use of f=0.8 resulted in det(**R**) exceeding the upper bound criterion, Eq. (10), for some elements.

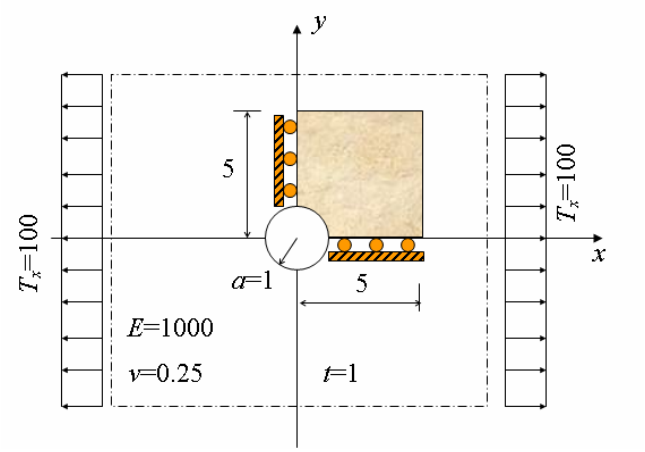

Fig. 8 An infinite plate with a circular hole

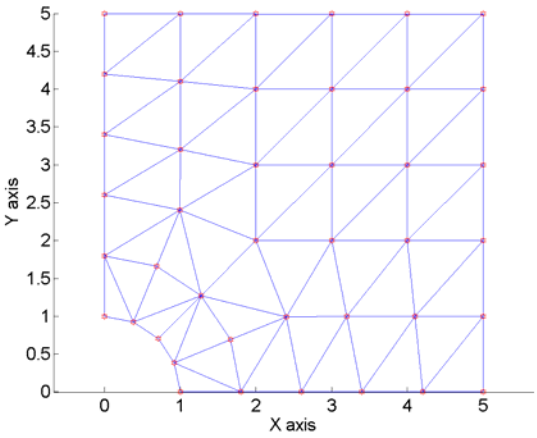

Fig. 9 Initial mesh for the holed plate

The convergence characteristics for displacement and strain energy are shown in Figs. 10 and 11, respectively. The figures show that the rates of convergence of all K-FEM options are nearly equal, for displacement as well as strain energy. The fastest convergence rate in term of displacement error is achieved by the K-FEM with P3-3-G80 (the rate, R=2.60) while the fastest one in term of strain energy error is the K-FEM with P3-3-QS (R=1.37). Theoretically, the accuracy and convergence rate of the K-FEM with cubic basis are higher than those with quadratic basis. However, this is not the case here because of the incompatibilities of the K-FEM.

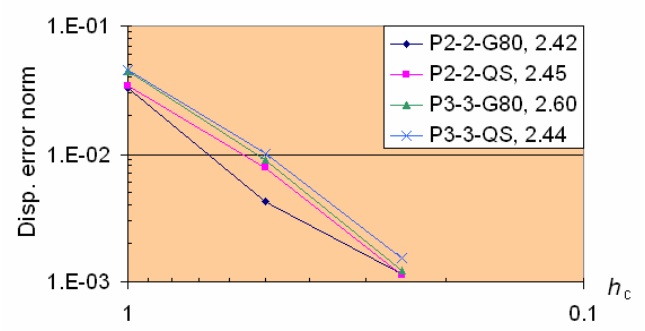

Fig. 10 Relative displacement error norms vs. element characteristic size for the holed plate

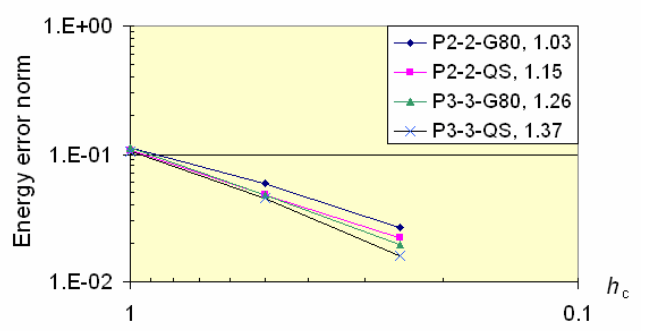

Fig. 11 Relative errors of strain energy vs. element characteristic size for the holed plate

CONCLUSIONS

Convergence characteristics of the K-FEM with different options have been studied in the context of plane stress and Reissner-Mindlin plate problems. The K-FEMs considered passed the weak patch tests except for the K-FEM with option P3-3-G0. For the K-FEM with the Gaussian correlation function, the convergence characteristics were better as the correlation parameter higher. The K-FEM with the QS correlation function generally had better convergence characteristics than that with the Gaussian. The incompatibility of the K-FEM tended to decrease as the mesh was refined. The adverse effect of the incompatibility was that the convergence rate for the K-FEM with a higher order basis function might not be faster.

Since the solutions of the K-FEM with the QS correlation function showed very good convergence characteristics, the use of the QS correlation function in a K-FEM for analyses two-dimensional problems is recommended. With this study, it is confirmed that the K-FEM is a viable alternative to the standard

FEM and has great potential in engineering applications. Future research should be directed at: (1) convergence study of the K-FEM for three-dimensional problems, and (2) extension and application of the K-FEM to different problems in engineering.

REFERENCES

[1] G.R. Liu, *Mesh Free Methods*, CRC Press, Boca Raton, USA (2003).

[2] Y.T. Gu, *Meshfree methods and their comparisons*, Int. J. Comput. Meth., 2, (2005), 477-515.

[3] T. Belytschko, Y.Y. Lu, L. Gu, *Element-free Galerkin methods*, Int. J. Num. Meth. Eng., 37, (1994), 229-256.

[4] K. Plengkhom, W. Kanok-Nukulchai, *An enhancement of finite element methods with moving Kriging shape functions*, Int. J. Comput. Meth., 2, (2005), 451-475.

[5] L. Gu, *Moving Kriging interpolation and element-free Galerkin method*, Int. J. Num. Meth. Eng., 56, (2003), 1-11.

[6] F.T. Wong, W. Kanok-Nukulchai, *A Kriging-based finite element method for 2D elastostatics*, to be submitted to Int. J. Num. Meth. Eng. (2007).

[7] K.Y. Dai, G.R. Liu, K.M. Lim, Y.T. Gu, *Comparison between the radial point interpolation and the Kriging interpolation used in meshfree methods*, Comput. Mech., 32, (2003), 60-70.

[8] F.T. Wong, W. Kanok-Nukulchai, *Kriging-based finite element method for analyses of Reissner-Mindlin plates*, in W. Kanok-Nukulchai, S. Munasinghe, N. Anwar eds. *Emerging Trends*: *Keynote Lectures and Symposia*. *Proc. 10th East-Asia Pacific Conf. Struct. Eng. Const.*, *Bangkok*, *3-5 August 2006*, ACECOMS, Pathumthani, Thailand (2006), pp. 509-514.

[9] R.A. Olea, *Geostatistics for Engineers and Earth Scientists*, Kluwer Academic Publishers, Boston, USA (1999).

[10] H. Wackernagel, *Multivariate Geostatistics*, 2nd edition, Springer, Berlin, Germany (1998).

[11] H. Noguchi, T. Kawashima, T. Miyamura, *Element free analyses of shell and spatial structures*, Int. J. Num. Meth. Eng., 47, (2000), 1215-1240.

[12] O.C. Zienkiewicz and R.L. Taylor, *The Finite Element Method*, vol. 1: The Basis, 5th edition, Butterworth Heinemann, Oxford, England (2000).

[13] A. Razzaque, *The patch test for elements*, Int. J. Num. Meth. Eng., 22, (1986), 63-71.

[14] R.D. Cook, D.S. Malkus, M.E. Plesha, R.J. Witt, *Concepts and Applications of Finite Element Analysis*, 4th edition, John Wiley and Sons, Madison, USA (2002).

[15] R.H. MacNeal, R.L. Harder, *A proposed standard set of problems to test finite element accuracy*, Finite Elements in Analysis and Design, 1, (1985). 3-20.

[16] F.T. Wong, W. Kanok-Nukulchai, *A Kriging-based finite element method for analyses of Reissner-Mindlin plates*, to be submitted to Comput. Methods Appl. Mech. Engrg. (2007).

[17] J.L. Batoz, I. Katili, *On a simple triangular Reissner/Mindlin plate element based on incompatible modes and discrete constraints*, Int. J. Num. Meth. Eng., 35, (1992), 1603-1632.

[18] P. Tongsuk, W. Kanok-Nukulchai, *Further investigation of element-free Galerkin method using moving Kriging interpolation*, Int. J. Comput. Meth., 1, (2004), 345-365.